This is a preprint. Please check (and cite 😊) the accepted version at:

Chem. Commun., 2019,**55**, 12773-12776

DOI: 10.1039/C9CC05990C

https://doi.org/10.1039/C9CC05990C

The SI is attached at the end of this file.

SI videos are available at:

https://hagayshpaisman.wixsite.com/shpaismanlab/copy-of-videos

Simultaneous laser-induced synthesis and micro-patterning of a metal organic framework

Nina Armon,[a,b] Ehud Greenberg,[a,b] Eitan Edri,[a,b] Avraham Kenigsberg,[a,b] Silvia Piperno,[a,b] Omree Kapon,[a,b] Ohad Fleker,[a] Ilana Perelshtein,[b] Gili Cohen-Taguri,[b] Idan Hod[c] and Hagay Shpaisman[a,b,*]

Micro-patterning of a metal organic framework (MOF) from a solution of precursors is achieved by local laser heating. Nano-sized MOFs are formed, followed by rapid assembly due to convective flows around a heat-induced micro-bubble. This laser-induced bottom-up technique is the first to suggest simultaneous synthesis and micro-patterning of MOFs, alleviating the need for pre-preparation and stabilization.

Metal-organic frameworks (MOFs) are compounds comprising metal ions coordinated to organic ligands that have attracted substantial attention during the last two decades due to their controlled porosity,[1] high surface area,[2] and electrochemical properties.[3] MOFs are suggested for gas storage[4] and separation,[5] catalysis,[6,7] and electrochemical applications.[8] Patterning of MOFs is required for many applications in the fields of sensing[9] and microelectronics.[10] Recently, various methods were demonstrated for MOF patterning[11] such as electrophoretic deposition,[12] ink-jet printing,[13] and various lithography derivatives.[14] Each of these methods has some limitations, for example lithography requires a photoresist and masks, while ink-jet printing offers a minimum feature size of tens of microns and requires pre-preparation of the MOF material with added stabilizers.[13] Therefore, there is constant pursuit of additional micro-patterning methods that could address the limitations of current methods.

Here, we demonstrate a method for micro-patterning of MOFs utilizing the modulated laser-induced micro bubble technique (M-LIMBT). This approach yields higher resolution than ink-jet printing and does not require pre-preparation, as the MOFs, are simultaneously synthesized and patterned. Previous laser-based studies have only shown post-processing of MOFs, accomplished by taking a pre-synthesized MOF crystal and micro-patterning it with metals[10] and fluorescent materials.[15] LIMBT was shown to micro-pattern various nanoparticles (NPs)[16–19] by using a continuous wave (CW) laser that heats NPs in a dispersion close to the substrate, increasing the vapor pressure of the surrounding medium until a microbubble is formed. The surface tension at the heated area around the microbubble/substrate interface is substantially decreased and produces strong shear forces along the microbubble surface that drag the surrounding fluid.[20] These Marangoni convection flows carry the NPs to the microbubble/substrate interface where some of them are pinned. Once the microscope stage is moved, the microbubble follows the laser focal point, resulting in deposition along a pre-determined path. It has been recently shown[21] that modulating the laser (M-LIMBT) improves certain characteristics of the formed deposition such as its continuity and minimal feature size. This method

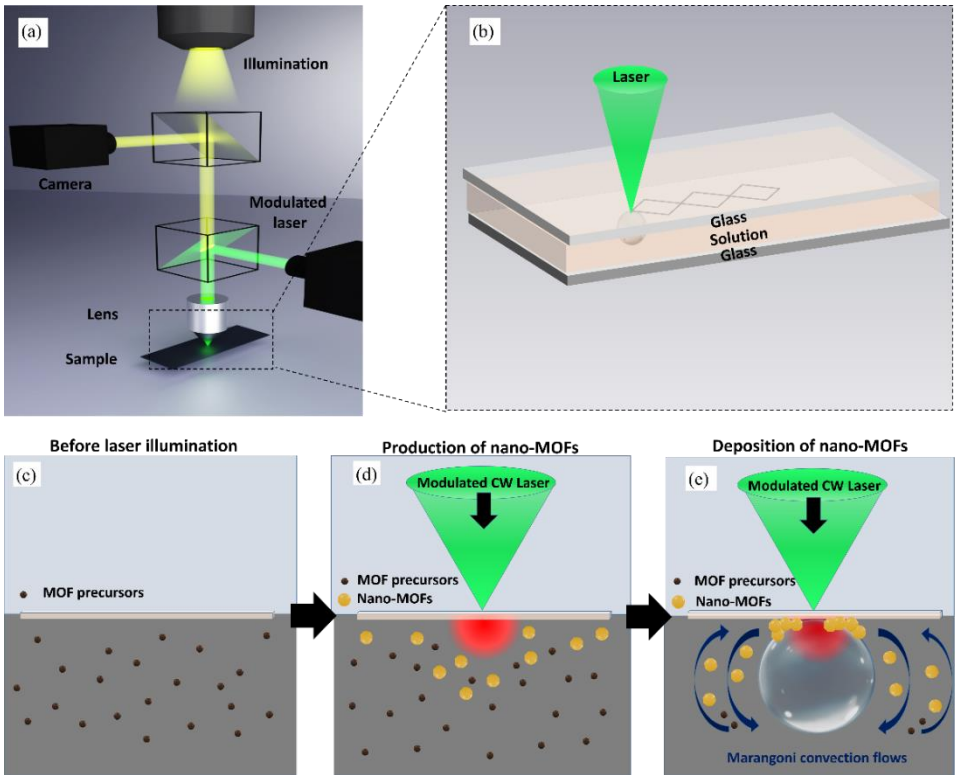

Fig. 1: (a) Illustration of the optical setup: a modulated laser beam is relayed to the objective lens by a dichroic mirror, and the lens focuses the laser on the (b) upper substrate/liquid interface of a solution containing MOF precursors. The solution (c) is heated by the laser, producing nano-MOFs (d) and increasing the vapor pressure until a microbubble is formed and convection flows carry the nano-MOFs, some of which are pinned (e) at the solution/microbubble/substrate interface. By moving the stage relative to the focal point, MOFs with continuous micro-patterns are formed.

has been further expanded to include deposition of metals and metal oxides from a precursor solution.[22–24] In these cases, the laser initially heats the precursors to form NPs by photo-thermal reaction, followed by their deposition as discussed above.

We first demonstrate micro-patterning of MOFs by applying M-LIMBT to a solution of precursors (metal ions and ligands). The deposits were analysed by EDS, XRD, HRTEM, Raman and FTIR spectroscopy to verify the presence of an iron-based MOF. Finally, we determine the deposition mechanism and demonstrate control over the width and height of the deposits. This laser-induced bottom-up technique is the first to suggest simultaneous synthesis and micro-patterning[25,26] of MOFs, thus pre-preparation and stabilization are not required.

As a model system we chose an iron based MOF in which the laser supplies the heat required by its synthesis.[27–30] The metal precursor was iron(III) acetylacetonate, while the source of the ligand was 1,3,5-benzenetricarboxylic acid (trimesic acid). The solution was prepared by mixing both precursors at room temperature in N,N-dimethylformamide (DMF). Additives were avoided, as the MOFs produced were shown to form even at room temperature in acidic[31] or basic[32,33] conditions, which would be unfavourable, as the reaction would occur beyond the laser focal point. The solution was stirred for 30 minutes and then inserted between two thin (~100 µm) glass slides (Fig. 1b & 1c).

The optical setup consisted of a modulated (1 kHz, 20% duty cycle) 532 nm CW laser relayed by a dichroic mirror to an objective lens of a microscope (Fig. 1a). The experiments were recorded by a CMOS camera, and the stage of the microscope was computer-controlled to move along a predetermined path at a stage velocity of 10 µm/s. The laser power was 1.3 mW unless otherwise stated and was focused at the interface between the upper glass slide and the solution.

The laser light is absorbed by the precursors in the solution, generating heat and producing nano-MOFs (Fig. 1d, Fig. 4a and Video SV1). The vapor pressure of the solvent increases and eventually becomes sufficiently high to support the formation of a microbubble. The resultant temperature gradient between the upper and lower parts of the microbubble leads to a surface tension gradient that promotes Marangoni convection flows, which also carry the nano-MOFs towards the solution/microbubble/substrate interface where some of them are pinned (Fig. 1e). Upon moving the microscope stage, the microbubble follows the laser spot, resulting in continuous pinning of material along the path to produce the desired micro-structure (Fig. 2a–c and Video SV2). Energy dispersive X-ray spectrometry (EDS) revealed that the deposition consists of iron and carbon (Fig. 2d & e, respectively). The iron is attributed to the metal atom of the formed MOF, while the carbon is ascribed to the organic ligand (H_3BTC, trimesic acid). Topography of the micro-patterned surface obtained by an optical profilometer is provided in Fig. 2f.

To confirm that the micro-patterned structures are indeed MOFs, we characterized them using several methods. Previous studies have shown that there are two types of MOFs that could be formed by these precursors: MIL-100(Fe) and FeBTC.[34–36] MIL-100(Fe) has a crystalline cubic structure with a $Fd\bar{3}m$ space group, while FeBTC has significantly lower crystallinity and is considered semi

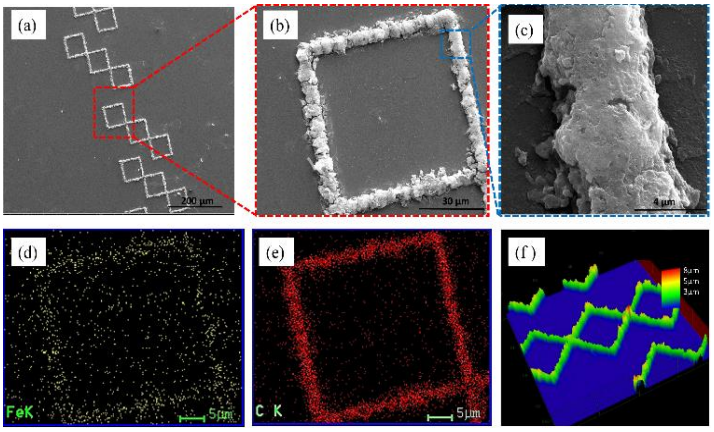

Fig. 2: SEM micrographs of MIL-100(Fe) micro-pattern at various magnifications (a)–(c), EDS mappings of iron (d) and carbon (e), and surface topography obtained by optical profilometer (f).

amorphous. While some of the following characterization methods (such as FTIR and Raman) can't distinguish between these MOFs, diffraction methods do not support the presence of a fully crystalline structure.

The X-ray diffraction (XRD) spectrum of a micro-pattern is shown in Figure 3a, and is with good agreement with previous XRD measurements of FeBTC[28–30,32,33,37,38] demonstrating peaks around 2Θ of ~3.9°, 6.5°, 11°, 19° and 24°. In addition, there is no indication of the presence of any other phases, e.g., iron oxides. We note, that MIL-100(Fe) has sharp peaks at similar angles.[35,39–42] Therefore, it could be rationalized that due to the small size of the nano MOFs (see Fig. 4a) broadening of the peaks could occur.[31] However, selected area diffraction pattern (SADP)[43] measurements on these nano MOFs at the HRTEM (Fig. S1 in SI) did not demonstrate a crystallite structure that would be expected by MIL-100(Fe). EDS measurements reveal the presence of both Fe and C (Fig. S1e in SI), in accordance with an Iron based MOF.

The Fourier transform infra-red (FTIR) spectrum show in Fig. 3b correlates well with the literature data for FeBTC and MIL-100(Fe).[27,37,38,40–42,44] The peaks at 538, 614, are assigned to C-H bending vibrations of benzene, the peak at 936 cm^{-1} is attributed to Fe-OH vibrations, those at 1109 and 1264 cm^{-1} arise from C-O vibrations, and the peaks at 1367 and 1442 cm^{-1} correspond to O-C-O vibrations. The peaks at 1558 and 1615 cm^{-1} arise from C=C and C=O vibrations, the peak at 1699 cm^{-1} is attributed to C=O vibrations, and the broad peak at 3075 cm^{-1} corresponds to O-H stretching. Finally, the Raman spectrum (Fig. 3c) was in agreement with the reported spectrum of these MOFs.[30,44,45] The peaks at 1243 and 1610 cm^{-1} correspond to C=O and C-O stretching, while those at 1474, 1375 and 1006 cm^{-1} correspond to vibrations of benzene rings.[46] The agreement of our measurements with literature data (XRD, EDS, Raman and FTIR) provides strong indication that the deposited micro-patterns consist of a semi crystalline iron-based MOF (FeBTC).

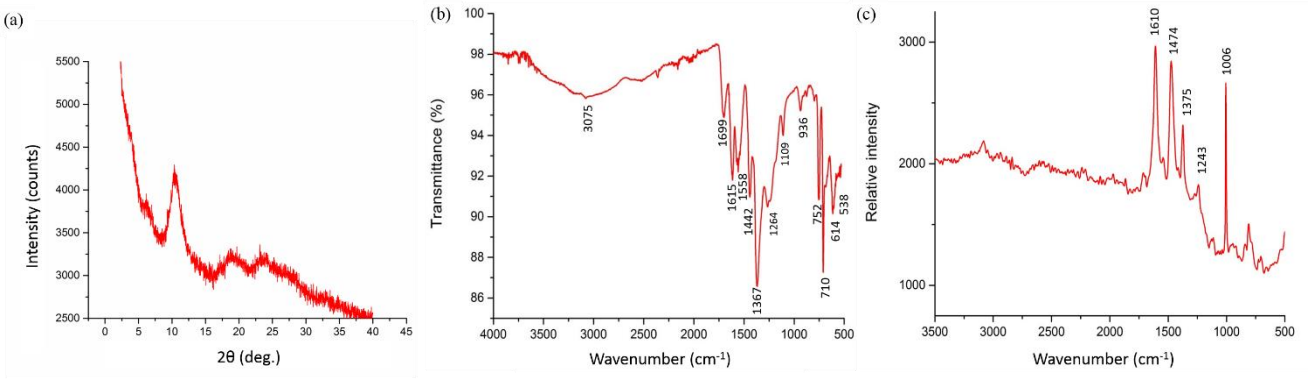

Fig. 3: Spectra of micro-patterned MOF: (a) XRD, (b) FTIR and (c) Raman.

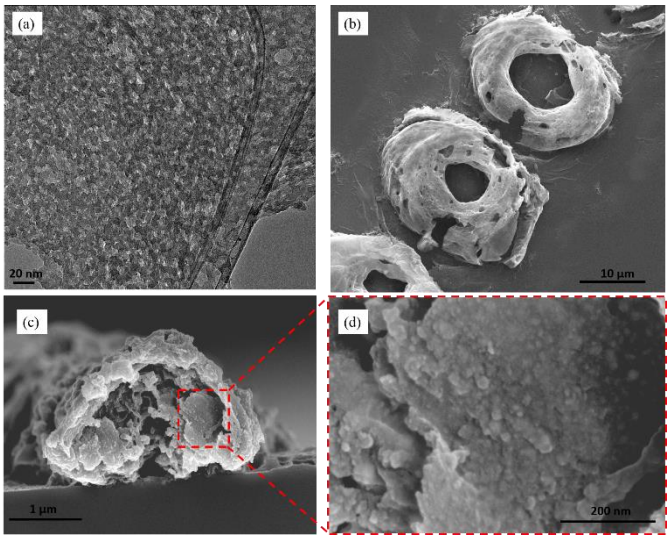

Fig. 4. (a) HRTEM micrograph of nano-MOFs synthesized by laser illumination (5 min). (b) SEM micrograph of deposition by short laser exposures (0.34 s). Ring-shaped patterns indicate that nano-MOFs were deposited along the contact area between the microbubble and the substrate. (c), (d) HRSEM image of a cross-section of micro-patterned MOF.

Confirmation of the deposition mechanism outlined above – formation of nano-MOFs that are deposited by M-LIMBT – was found by production of nano-MOFs when the laser is not focused on the substrate. Video SV1 shows the appearance of a blurry cloud when the laser is focused at the center of the solution (>50 µm away from the substrate and air). After five minutes of exposure, the formed material was transferred to a carbon-coated copper TEM grid. TEM imaging revealed particles that are ~10 nanometers in diameter (Fig. 4a). HRSEM images of a cross-section of material deposited by laser focusing on the substrate (Fig. 4c & d) revealed an accumulation of NPs. The driving force for this accumulation was determined by studying depositions formed at relatively short times. This was achieved by a mechanical shutter along the laser path that was set to open for 0.34 s and then remain closed for 0.44 s. As can be seen in the SEM image at Fig. 4b, the formed deposition is ring shaped. As shown previously,[17,21,22] ring-shaped patterns are the fingerprints of microbubble-assisted deposition, as the spherical bubble promotes deposition at its contact area with the substrate.

Finally, we demonstrate control the deposition width and height by changing the incident laser intensity between 1.3 and 10.6 mW; deposition was not observed below 1.3 mW, while at intensities above 10.6 mW, the increased heating sometimes led to extensive solvent evaporation. As shown in Fig. 5, higher intensity leads to extensive material deposition with increase in both width and height due to availability of more energy for production of nano-MOFs, followed by stronger heating that forms enlarged micro-bubbles with increased temperature gradient.

In conclusion, simultaneous synthesis and micro-patterning of an iron-based MOF was demonstrated by a laser-induced method. The laser light is absorbed by a solution of precursors, producing heat that results in both formation of nano-MOFs and elevation of the solution vapor pressure to eventually generate a microbubble. Marangoni convection flows carry the nano-MOFs towards the solution/microbubble/substrate interface, where some are pinned. By moving the microscope stage, arbitrary shaped micro-patterns were formed. This approach does not require pre-preparation or stabilization of MOFs and could be applicable for sensor formation and microelectronic devices.

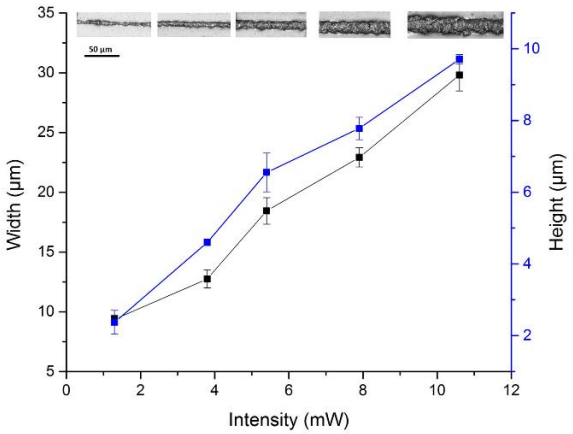

Fig. 5: Width and height of micro-patterned MOF (above) as a function of laser intensity.

The authors acknowledge Dr. Yuval Elias for scientific editing, and Dr. Sharon Bretler for assistance with HRSEM. The authors thank Bar-Ilan University for the generous start-up package.

Conflicts of interest

There are no conflicts to declare.

Notes and references

1 P. Horcajada, C. Serre, G. Maurin, N. A. Ramsahye, F. Balas, M. Vallet-Regí, M. Sebban, F. Taulelle and G. Férey, *J. Am. Chem. Soc.*, 2008, **130**, 6774–6780.
2 H. Furukawa, N. Ko, Y. B. Go, N. Aratani, S. B. Choi, E. Choi, A. O. Yazaydin, R. Q. Snurr, M. O'Keeffe, J. Kim and O. M. Yaghi, *Science*, 2010, **329**, 424–428.
3 L. Sun, M. G. Campbell and M. Dincă, *Angew. Chem. Int. Ed.*, 2016, **55**, 3566–3579.
4 K. Sumida, D. L. Rogow, J. A. Mason, T. M. McDonald, E. D. Bloch, Z. R. Herm, T.-H. Bae and J. R. Long, *Chem. Rev.*, 2012, **112**, 724–781.
5 J.-R. Li, J. Sculley and H.-C. Zhou, *Chem. Rev.*, 2012, **112**, 869–932.
6 M. Yoon, R. Srirambalaji and K. Kim, *Chem. Rev.*, 2012, **112**, 1196–1231.
7 H. He, J. A. Perman, G. Zhu and S. Ma, *Small*, 2016, **12**, 6309–6324.
8 A. Morozan and F. Jaouen, *Energy Environ. Sci.*, 2012, **5**, 9269.
9 M. G. Campbell, S. F. Liu, T. M. Swager and M. Dincă, *J. Am. Chem. Soc.*, 2015, **137**, 13780–13783.
10 R. Ameloot, M. B. J. Roeffaers, G. De Cremer, F. Vermoortele, J. Hofkens, B. F. Sels and D. E. De Vos, *Adv. Mater.*, 2011, **23**, 1788–1791.
11 P. Falcaro, R. Ricco, C. M. Doherty, K. Liang, A. J. Hill and M. J. Styles, *Chem Soc Rev*, 2014, **43**, 5513–5560.
12 I. Hod, W. Bury, D. M. Karlin, P. Deria, C.-W. Kung, M. J. Katz, M. So, B. Klahr, D. Jin, Y.-W. Chung, T. W. Odom, O. K. Farha and J. T. Hupp, *Adv. Mater.*, 2014, **26**, 6295–6300.
13 J.-L. Zhuang, D. Ar, X.-J. Yu, J.-X. Liu and A. Terfort, *Adv. Mater.*, 2013, **25**, 4631–4635.
14 C. M. Doherty, G. Grenci, R. Riccò, J. I. Mardel, J. Reboul, S. Furukawa, S. Kitagawa, A. J. Hill and P. Falcaro, *Adv. Mater.*, 2013, **25**, 4701–4705.
15 J. Yu, Y. Cui, C.-D. Wu, Y. Yang, B. Chen and G. Qian, *J. Am. Chem. Soc.*, 2015, **137**, 4026–4029.
16 B. Bangalore Rajeeva, L. Lin, E. P. Perillo, X. Peng, W. W. Yu, A. K. Dunn and Y. Zheng, *ACS Appl. Mater. Interfaces*, 2017, **9**, 16725–16733.
17 S. Fujii, K. Kanaizuka, S. Toyabe, K. Kobayashi, E. Muneyuki and M. Haga, *Langmuir*, 2011, **27**, 8605–8610.
18 B. Roy, M. Arya, P. Thomas, J. K. Jürgschat, K. Venkata Rao, A. Banerjee, C. Malla Reddy and S. Roy, *Langmuir*, 2013, **29**, 14733–14742.
19 Y. Xie and C. Zhao, *Nanoscale*, 2017, **9**, 6622–6631.
20 K. Namura, K. Nakajima, K. Kimura and M. Suzuki, *Appl. Phys. Lett.*, 2015, **106**, 043101.
21 N. Armon, E. Greenberg, M. Layani, Y. S. Rosen, S. Magdassi and H. Shpaisman, *ACS Appl. Mater. Interfaces*, 2017, **9**, 44214–44221.
22 E. Greenberg, N. Armon, O. Kapon, M. Ben-Ishai and H. Shpaisman, *Adv. Mater. Interfaces*, 2019, 1900541.
23 S. Fujii, R. Fukano, Y. Hayami, H. Ozawa, E. Muneyuki, N. Kitamura and M. Haga, *ACS Appl. Mater. Interfaces*, 2017, **9**, 8413–8419.
24 L. D. Zarzar, B. S. Swartzentruber, B. F. Donovan, P. E. Hopkins and B. Kaehr, *ACS Appl. Mater. Interfaces*, 2016, **8**, 21134–21139.
25 S. Piperno, H. Sazan and H. Shpaisman, *Polymer*, 2019, **173**, 20–26.
26 I. Jacob, E. Edri, E. Lasnoy, S. Piperno and H. Shpaisman, *Soft Matter*, 2017, **13**, 706–710.
27 F. Zhang, J. Shi, Y. Jin, Y. Fu, Y. Zhong and W. Zhu, *Chem. Eng. J.*, 2015, **259**, 183–190.
28 T. Araya, C. Chen, M. Jia, D. Johnson, R. Li and Y. Huang, *Opt. Mater.*, 2017, **64**, 512–523.
29 N. Torres, J. Galicia, Y. Plasencia, A. Cano, F. Echevarría, L. F. Desdin-Garcia and E. Reguera, *Colloids Surf. Physicochem. Eng. Asp.*, 2018, **549**, 138–146.
30 L. Peng, S. Wu, X. Yang, J. Hu, X. Fu, M. Li, L. Bai, Q. Huo and J. Guan, *New J. Chem.*, 2017, **41**, 2891–2894.
31 P. Horcajada, S. Surblé, C. Serre, D.-Y. Hong, Y.-K. Seo, J.-S. Chang, J.-M. Grenèche, I. Margiolaki and G. Férey, *Chem Commun*, 2007, 2820–2822.

32 F. Martínez, P. Leo, G. Orcajo, M. Díaz-García, M. Sanchez-Sanchez and G. Calleja, *Catal. Today*, 2018, **313**, 6–11.
33 M. Sanchez-Sanchez, I. de Asua, D. Ruano and K. Diaz, *Cryst. Growth Des.*, 2015, **15**, 4498–4506.
34 A. Dhakshinamoorthy, M. Alvaro, P. Horcajada, E. Gibson, M. Vishnuvarthan, A. Vimont, J.-M. Grenèche, C. Serre, M. Daturi and H. Garcia, *ACS Catal.*, 2012, **2**, 2060–2065.
35 K. Guesh, C. A. D. Caiuby, Á. Mayoral, M. Díaz-García, I. Díaz and M. Sanchez-Sanchez, *Cryst. Growth Des.*, 2017, **17**, 1806–1813.
36 M. Rivera-Torrente, M. Filez, R. Hardian, E. Reynolds, B. Seoane, M.-V. Coulet, F. E. Oropeza Palacio, J. P. Hofmann, R. A. Fischer, A. L. Goodwin, P. L. Llewellyn and B. M. Weckhuysen, *Chem. - Eur. J.*, 2018, **24**, 7498–7506.
37 X. Hu, X. Lou, C. Li, Y. Ning, Y. Liao, Q. Chen, E. S. Mananga, M. Shen and B. Hu, *RSC Adv.*, 2016, **6**, 114483–114490.
38 E. García, R. Medina, M. Lozano, I. Hernández Pérez, M. Valero and A. Franco, *Materials*, 2014, **7**, 8037–8057.
39 S. Hindocha and S. Poulston, *Faraday Discuss.*, 2017, **201**, 113–125.
40 S. Taherzade, J. Soleimannejad and A. Tarlani, *Nanomaterials*, 2017, **7**, 215.
41 A. García Márquez, A. Demessence, A. E. Platero-Prats, D. Heurtaux, P. Horcajada, C. Serre, J.-S. Chang, G. Férey, V. A. de la Peña-O'Shea, C. Boissière, D. Grosso and C. Sanchez, *Eur. J. Inorg. Chem.*, 2012, **2012**, 5165–5174.
42 M. Nehra, N. Dilbaghi, N. K. Singhal, A. A. Hassan, K.-H. Kim and S. Kumar, *Environ. Res.*, 2019, **169**, 229–236.
43 X. Gong, H. Noh, N. C. Gianneschi and O. K. Farha, *J. Am. Chem. Soc.*, 2019, **141**, 6146–6151.
44 M. R. Lohe, M. Rose and S. Kaskel, *Chem. Commun.*, 2009, 6056.
45 H. Lv, H. Zhao, T. Cao, L. Qian, Y. Wang and G. Zhao, *J. Mol. Catal. Chem.*, 2015, **400**, 81–89.
46 J.-G. Lee, B. N. Joshi, E. Samuel, S. An, M. T. Swihart, J. S. Lee, Y. K. Hwang, J.-S. Chang and S. S. Yoon, *J. Alloys Compd.*, 2017, **722**, 996–1001.

Electronic Supplementary Information

Simultaneous laser-induced synthesis and micro-patterning of a metal organic framework

Nina Armon,[a,b] Ehud Greenberg,[a,b] Eitan Edri,[a,b] Avraham Kenigsberg,[a,b] Silvia Piperno,[a,b] Omree Kapon,[a,b] Ohad Fleker,[a] Ilana Perelshtein,[b] Gili Cohen-Taguri,[b] Idan Hod[c] and Hagay Shpaisman[a,b,*]

[a] Department of Chemistry, Bar-Ilan University, Ramat Gan 5290002, Israel

[b] Institute for Nanotechnology and Advanced Materials, Bar-Ilan University, Ramat Gan, 5290002, Israel

[c] Department of Chemistry and Ilse Katz Institute for Nanoscale Science and Technology, Ben-Gurion University of the Negev, Beer-Sheva 8410501, Israel

* hagay.shpaisman@biu.ac.il

Experimental section

Sample preparation. The solution containing the precursors was prepared by dissolving 0.134 g of iron(III) acetylacetonate (Stream Chemical, Inc.) and 0.063 g of 1,3,5-benzenetricarboxylic acid (trimesic acid, Aldrich) in 1 ml of N,N-dimethylformamide (DMF, Daejung). The solution was stirred for 30 minutes at room temperature. Samples were prepared by placing two clean standard microscope cover slips (#0, 100 µm thick), one on top of the other, with a Parafilm™ tape as a spacer. The solution was inserted between the two cover slips by capillary forces.

Optical setup. The optical setup (illustrated in **Figure 1a**) consists of a CW laser (532 nm, MGL-N-532A-4W, CNI) that is relayed by a dichroic mirror to an objective lens of a microscope (Nikon ECLIPSE LV100ND). We used a 50× (TU Plan ELWD, 0.6 NA, Nikon) objective lens. Modulation of the laser was performed by electrical means – controlling the power delivered to the laser diode – using transistor-transistor-logic (TTL) modulation (part of the laser driver circuit). The square-wave signal for the TTL modulation was generated by a Siglent function generator (SDG 5162). The laser power was set to 1.3 mW (unless stated otherwise) with a modulation of 20% duty cycle and a frequency of 1 kHz. The reported laser intensity was measured after the objective lens with a power meter (PM100, Thorlabs) while applying the modulation. A mechanical shutter (SH05, Thorlabs) was used for achieving the ring formations in **Figure 4b**. The microscope stage was computer-controlled with a velocity of 10 µm/s, and the experiments were

recorded by a CMOS camera (DPCAM, DeltaPix). We note that the micro-patterning of MOFs is not limited to setups where the laser is directed from above the sample. We achieved almost identical results when micro-patterning was formed on the bottom cover slip, with another optical setup based on an inverted microscope (Nikon, Eclipse Ti-U) using a 532 nm CW laser (DPSS laser, 5-532-DPSS-0.5-LN, Verdi) modulated by an optical chopper (MC1F100, Thorlabs). For simplicity and clarity, we focus our report on the first setup discussed above based on an upright microscope.

Characterization methods. X-ray diffraction (XRD) measurements were obtained using a Rigaku SmartLab X-ray diffractometer with Cu-Kα radiation (λ = 1.5406 Å, 40 kV and 30 mA) utilizing parallel beam optics. The scanned 2θ range was 2–40° with a step size of 0.02° and rate of 0.5 °/min.

Micro Raman measurements were performed using a confocal Raman microscope with 532 nm laser excitation, a 100× objective, a 100 µm confocal pinhole, and a 600 groves/mm grating (LabRAM HR, Horiba Jobin Yvon Corporation). The laser power was 60 mW, and a neutral density filter of optical density 1 was inserted in the beam path to prevent optical damage to the sample. The acquisition time was 30 s per scanning interval (~500 cm^{-1}), with all measurements taken in air at room temperature. IR transmission measurements were performed using a Nicolet iS10 FTIR system.

The samples for XRD, Raman and FTIR were prepared by micro-patterning many individual lines of MOFs on a glass slide with minimal spacing in-between lines to form a ~500 µm × 2 cm sample with laser intensity of 10.6 mW.

SEM images were obtained using a Quanta FEG 250 System with a built-in energy dispersive X-ray spectroscopy (EDS) system. HRSEM images were obtain by a FEI, Magellan 400L system. The preparation of samples imaging the cross-section of the micro-patterned MOF (**Figure 4c & 4d**) was performed by breaking the cover slip with the deposited material at selected locations, determined by scratching with a diamond knife (without physically touching the deposits). HRTEM images were obtained using a JEOL-2100 operated at 200 KeV, and the elemental analysis was conducted by Energy Dispersive X-ray Spectroscopy (EDS). For HRTEM measurements, the solution was prepared as described above, followed by diluting with DMF and filtration with a hydrophobic 0.22 µm PTFE syringe filter. A droplet (~100 µL) was positioned on a glass slide and held in place by capillary forces. After five minutes of laser illumination (at 10.6 mW), a TEM grid (Lacey carbon, 300 mesh copper grid, Ted Pella Inc.) was placed in contact with the bottom part of the droplet (at the solution/air interface) where the concentration of the formed nano-MOFs is maximal due to gravity. The TEM grid was washed with DMF and ethanol.

The measurements of the width and height of the deposits at different intensities were performed using an optical profilometer (LEXT OLS4100, Olympus). Each line was automatically averaged over >100 points. To obtain the data presented in **Figure 5**, for each reported intensity, three separate experiments were performed. In each experiment, five lines were deposited, thus each data point includes 15 individual measurements.

Author Contributions

Conceptualization, N.A, A.K., and H.S.; Investigation, N.A., E.G., O.K., O.F., I.P. and G.C.; Methodology, N.A., I.P., G.C., I.H. and H.S.; Formal analysis, N.A., I.P., G.C., I.H. and H.S. ; Funding acquisition, H.S.; Resources, H.S.; Supervision, I.H. & H.S.; Validation, N.A., E.E., S.P., I.H. and H.S.; Visualization, E.E. and N.A.; Writing – original draft, N.A., E.G. and H.S.; Writing – review & editing, N.A., E.G., I.P., G.C.,S.P., I.H. and H.S.;

Figure S1:

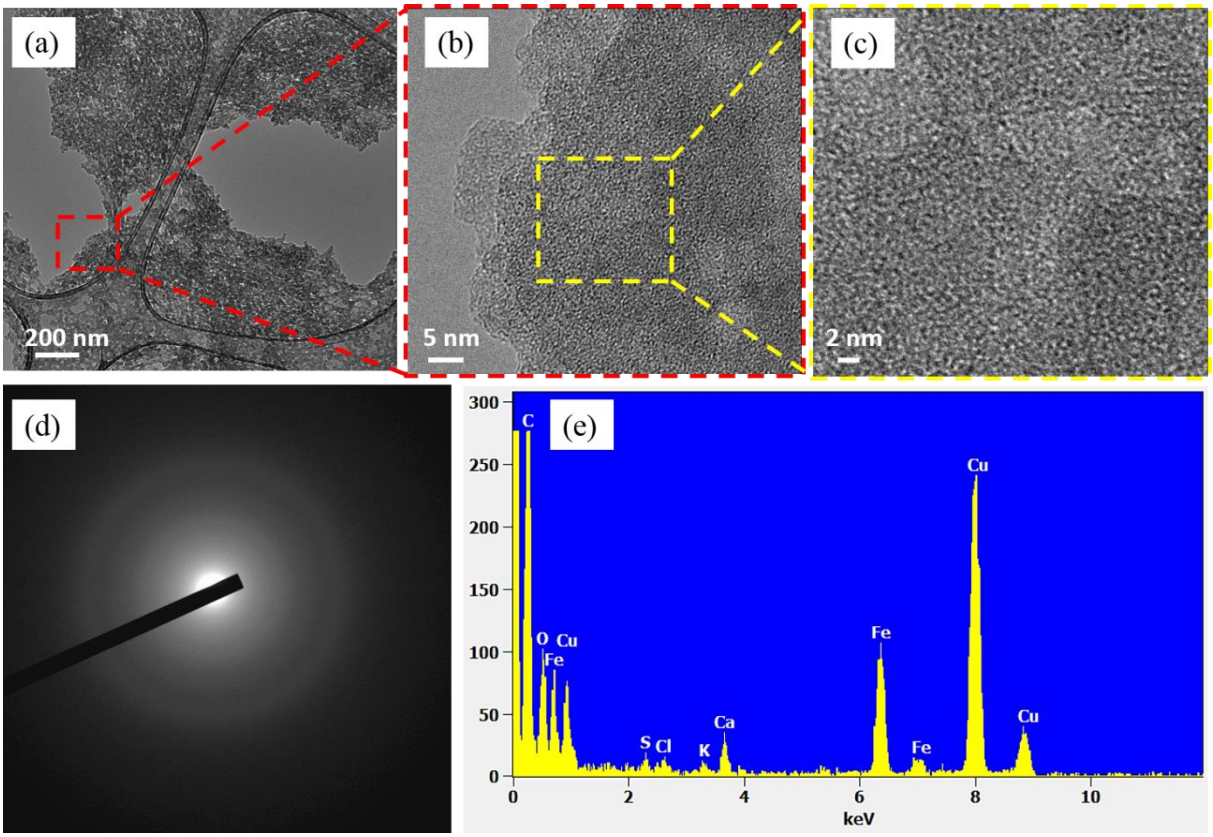

Fig. S2: (a-c) HRTEM images showing the formation of nano-MOFs. (d) SADP measurements of the iron-based MOF. (e) EDS spectrum verifying the presence of iron and carbon.

HRTEM images show that the laser indeed produces nano-MOFs (Fig. 4a and Fig. S1a-c). In addition, SADP measurements indicate that the fabricated nano-MOFs are amorphous (Fig.S1d). In addition, EDS spectrum (Fig.S1e) verifies the presence of iron, thus dismissing the option that only the BTC ligand is present.

Video SV1: laser synthesis of nano-MOFs.

Formation of nano-MOFs inside a droplet – a 1.3 mW laser beam was focused inside a droplet with MOF precursors, situated more than 50 μm away from the substrate. The solution immediately turned cloudy around the focal point.

Video SV2: micro-patterning by M-LIMBT.

Micro-pattern formation - by moving the microscope stage at a velocity of 10 μm/s along a predetermined path while the 1.3 mW laser beam was focused at the substrate/solution interface, continuous patterns of a MOF is formed. A micro-bubble is evident at the location of the laser focal point.